AAPS PharmSciTech, Vol. 10, No. 4, December 2009 (© 2009)
DOI: 10.1208/s12249-009-9313-3

Research Article

Effect of Particle Shape on Dry Particle Inhalation: Study of Flowability, Aerosolization, and Deposition Properties

Meer Saiful Hassan[1] and Raymond Wai Man Lau[1,2]

Received 20 May 2009; accepted 18 September 2009; published online 29 October 2009

Abstract. The shape effects of dry particles on flowability, aerosolization, and deposition properties in inhalation drug delivery are studied. The properties are compared with similar size range particles of different shapes such as sphere, needle, cube, plate, and pollen. Flowability of the particles is characterized by Carr's compressibility index and angle of slide (θ) method. The aerosolization and deposition properties of the particles are studied *in vitro* using an eight-stage Anderson cascade impactor with a Rotahaler®. Pollen-shaped particles are found to exhibit better flowability, higher emitted dose, and higher fine particle fraction than particles of other shapes in similar size range. They showed minimum θ of 35° and maximum emitted dose of 87% and fine particle fraction of 16%. The use of pollen-shaped particles can be a potential improvement in dry particle inhalation.

KEY WORDS: cascade impactor; dry particle inhalation; emitted dose; fine particle fraction; flowability; pollen-shaped particles.

INTRODUCTION

Pulmonary drug delivery has been gaining considerable interest as an effective and convenient alternative route of drug administration. The demand for more sophisticated drug formulation is increased for better delivery capacity and efficiency. Particles with an aerodynamic diameter (d_a) range of 1–5 μm were found to have the highest delivery efficiency (1,2). However, most studies are focused on spherical particles with various sizes to improve the delivery efficiency. Theoretically, different particle shapes can give rise to different drag forces and particle terminal settling velocities, which would in turn affect the aerodynamic behavior of the particles (1,3). A shape factor is normally used for non-spherical particles in the definition of aerodynamic diameter. Aerodynamic diameter is a general characterizing parameter for aerosol particles, defined as the diameter of a sphere of unit density that has the same terminal settling velocity as the particle under consideration:

$$d_a = d_g \sqrt{\frac{\rho_e}{\lambda \rho_s}} \tag{1}$$

where ρ_s=1 g/cm^3, d_g is the particle geometric diameter, ρ_e is the effective particle density in the same unit as ρ_s, and λ is the dynamic shape factor of the particle (1,2,4). This shape factor is defined as the ratio of the drag force of the particle to that of a sphere of equivalent volume (5). Increasing particle surface roughness would attribute to lower aerodynamic diameter (6). With a reduced aerodynamic diameter, particles would have a higher possibility of reaching the deep lung as compared with spherical particles. Indeed, researchers found that elongated particles exhibit better aerodynamic behavior than spherical particles (7–9). Elongated or needle-like particles are reported to have longer suspended time in the air and can travel further in the lung airway (9). However, high elongated particles also experience high interception deposition as demonstrated by Balásházy *et al.* (9).

Particle aerosolization is another important factor for deep lung delivery. Aerosolization of particles from the inhaler depends on the particle–particle and particle–wall interaction. Particle interaction is closely related to the van der Waals force, which is a function of the particle surface morphology (11,12), size (13), shape (12,14), electrostatic properties (15), and hygroscopicity (16). Particle shape that has low contact area and van der Waals force will have lower aggregation tendency and can be dispersed well in the air (17). Elongated particles are not suitable for aerosolization due to their large attractive forces (12).

[1] School of Chemical and Biomedical Engineering (SCBE), Nanyang Technological University (NTU), 62 Nanyang Drive, Singapore, 637459, Singapore.
[2] To whom correspondence should be addressed. (e-mail: wmlau@ntu.edu.sg)

NOMENCLATURE: A, Hamaker constant; d_a, Aerodynamic diameter; d_g, Geometric diameter; F, Van der Waals force between two spherical particles; H, Separation distance; R, Radius of the particles in interaction; R, Radius of the contact area of the two interacting particles; θ, Angle of slide; λ, Dynamic shape factor; ρ_{bulk}, Bulk density; ρ_e, Effective particle density; ρ_s, Unit density; ρ_{tap}, Tap density.

Most of the inhalation studies are focused on spherical particles and a few on elongated particles. It has been shown that particle shape has an important effect on dry powder inhalation (18). However, the use of shape factor is also not sufficient to represent the effect of shape on the particle aerodynamic behavior as it also depends on the particle orientation and the contact area with other particles. Therefore, the shape effect on these properties needs to be investigated properly to improve particle aerosolization and minimize early depositions due to interception, inertial impaction, and gravitational deposition. A preliminary study found that a pollen shape characteristic of particles can enhance the flowability, aerosolization, and deposition properties compared to particles having similar volume equivalent diameter (18). However, the particles' characteristic size and aerodynamic diameter are important factors for the aerodynamic behavior. Therefore, the particle shape effect on the flowability, aerosolization, and deposition behavior is investigated extensively in this study with the introduction of additional particles with different sizes and shapes. The particle shapes studied include sphere, plate, cube, needle, and pollen.

EXPERIMENTAL

Preparation

Pollen-shaped and spherical hydroxyapatite (HA, $Ca_5(PO_4)_3(OH)$) particles are synthesized using potassium dihydrogen phosphate (KH_2PO_4, Sigma-Aldrich), calcium nitrate tetrahydrate ($Ca(NO_3)_2{\cdot}4H_2O$, Sigma-Aldrich), poly (sodium-4-styrene-sulfonate) (PSS, Sigma-Aldrich), and urea (Sigma-Aldrich) (19). Thirty milliliters of KH_2PO_4 (0.02 M) solution is mixed with 50 ml of $Ca(NO_3)_2{\cdot}4H_2O$ (0.02 M) solution. PSS and urea are then added to the mixture. The amount of PSS and urea added govern the shape and size of the product HA particles. In this study, the PSS concentration used ranges from 40 to 80 g/l, and urea concentration used ranges from 3 to 7.5 M. The final mixture is stirred to completely dissolve the urea. The solution mixture is then kept in an oven at 200°C for 3–6 h to allow sufficient time for hydrothermal reaction. Finally, the precipitated product is filtered, washed, and then dried at 70°C (18).

Spherical calcium carbonate ($CaCO_3$) particles are produced by using $Ca(NO_3)_2{\cdot}4H_2O$, sodium carbonate (Na_2CO_3, Kanto Chemical), and PSS (20). Equal volume of 0.1 M $Ca(NO_3)_2{\cdot}4H_2O$ and 0.1 M Na_2CO_3 solution are mixed in a solution with PSS concentration of 50 g/l at room temperature. The $CaCO_3$ precipitate is then filtered, washed, and dried at 70°C.

Plate-shaped calcium oxalate (CaC_2O_4) particles are produced by precipitation reaction of sodium oxalate ($Na_2C_2O_4$, Kanto Chemical) and calcium chloride ($CaCl_2$, Kanto Chemical) using poly-(styrene-alt-maleic acid) (PSMA, Sigma-Aldrich) as the surfactant (21). 0.8 ml of $Na_2C_2O_4$ (0.1 M) solution is added to 80 ml aqueous solution of PSMA (0.5 g/l). Dilute HCl (Fluka) is added to achieve a pH of 4. 0.8 ml of $CaCl_2$ (0.1 M) is then added, and the mixture is kept at 25°C under static condition for 24 h. The product is then collected, washed, and dried at 70°C.

Cube-shaped $CaCO_3$ is produced by precipitation reaction of Na_2CO_3 and $CaCl_2$ using cetyl trimethylammonium bromide (CTAB) as the surfactant (22). Approximately 1.28 ml of Na_2CO_3 (0.5 M) solution is added to 80 ml aqueous solution of CTAB (1 g/l). NaOH (Fluka) is added to obtain a pH of 10. Approximately 1.28 ml of $CaCl_2$ (0.5 M) solution is added, and the mixture is kept at 80°C under static condition for 24 h before the final product is collected. After washing, the product is dried at 70°C.

Needle-shaped $CaCO_3$ particles are synthesized by precipitation reaction of potassium hydrogen carbonate ($KHCO_3$, Merck) and $CaCl_2$ (23). Equal volume of 0.1 M $KHCO_3$ and $CaCl_2$ are heated until boiling separately. The two solutions are then mixed together to obtain the carbonate precipitate. The precipitate is then filtered, washed, and dried at 110°C.

Particles of different materials could have difference in flowability, aerosolization, and deposition properties. These properties of particles highly depend on van der Waals forces between the particles. The van der Waals force between two equal size spherical particles can be calculated by the equation (12):

$$F = \frac{AR}{12H^2} + \frac{A}{6\pi H^3}\pi r^2 \tag{2}$$

where R is the diameter of the spherical particle, A is the Hamaker constant, H is the separation distance between two particle surfaces, and r is the radius of the contact area. Based on Eq. 2, the van der Waals force, F, is proportional to the first order of the Hamaker constant, A, but inversely proportional to second and third order of the separation distance, H. Visser (12) also showed that the separation distance have a stronger effect on the van der Waals force than the Hamaker constant. Therefore, even though particles of different materials are used in this study, the difference in flowability, aerosolization, and deposition properties can be considered to be solely dependent on the particle physical properties (size, shape, and density).

Mean Particle Diameter and Particle Shape

The particle sizes are measured by laser diffraction (LD, Malvern Mastersizer 2000). The samples are dispersed in 1% isopropyl alcohol (IPA) solution in distilled water using ultrasonication prior to the measurement. Laser diffraction size measurement for each sample is carried out three times. The size distribution determined by laser diffraction is volume-weighted and expressed in terms of $d(50\%)$.

Shape and size of the particles are also characterized using scanning electron microscope (SEM, JEOL JSM-5600). Dry particle samples are dispersed on a carbon tape that is attached on a stub. The particles are coated with platinum under an argon atmosphere (JEOL, JFC-1600, Auto Fine Coater) for 60 s with a current of 20 mA. Then, the coated particles are examined under SEM. The SEM images are taken randomly from different areas of the samples. The images are analyzed to obtain the size distribution of the particles. Dimensions of over 200 particles are measured for each sample. The surface morphologies of the particles are assessed qualitatively based on the SEM images.

Particle Density

Bulk (ρ_{bulk}) and tap (ρ_{tap}) densities are important properties for dry particle samples. ρ_{bulk} and ρ_{tap} of the experimental samples are measured according to Shi *et al.* (24). One hundred milligrams of a particle sample is measured on an analytical balance. A 1-ml micro-syringe tube containing the particles is then tapped against a tabletop by hand at a rate of about four times per second for 2,000–2,500 taps until no reduction of the particle volume is noticed. The measured density at $n=0$ is the bulk density and at $n=$ 2,000–2,500 is the tap density.

Powder Flowability

The flowability of each particle is analyzed by Carr's compressibility index (CI) and angle of slide (θ). CI is a common way to characterize the flow behavior of particles. CI can be determined based on the tap density (ρ_{tap}) and bulk density (ρ_{bulk}):

$$\mathrm{CI} = \frac{\rho_{tap} - \rho_{bulk}}{\rho_{tap}} \times 100\%. \quad (3)$$

Lower CI values are indicative of better flowability (25,26). CI indicates the compressibility of powders. Compressible powders have strong interparticle forces and would exhibit poor flowability (25). The characterization of particle flowability using CI is based on empirical understanding and may pose discrepancies in result interpretation. Therefore, flowability demonstration was also conducted by θ (27).

The angle of slide method is an effective method for the characterization of the flowability of powders (27). A volume of particle samples that is used in the capsule of the cascade impaction experiment is placed on a dry glass plate. A lab jack is used to tilt one side of the plate vertically upwards until the major portion of the powder slides. The angle between the tilted and horizontal planes (angle of slide, θ) is then measured. The lower the angle, the better is the flowability. Each sample is measured in triplicate. Statistical analysis of the results is performed by ANOVA. θ indicates the ability of the particles to flow in the presence of shear. This flowability is closely related to particle adhesion and directly affects the particle dispersibility and flow through inhalation system.

Preparation of Capsules

Twenty milligrams of each sample is loaded into a hard gelatin capsule (gelatin embedding capsules, size 4, 0.25 cc, Polysciences Inc.) manually.

In Vitro Aerosolization and Deposition Properties

An eight-stage Andersen cascade impactor (ACI, COPLEY Scientific) is used to determine the aerosolization and deposition properties *in vitro*. The experiment is carried out at an air flow rate of 30 l/min. In each experiment, 8 ml of the dissolving solvent (2% HNO_3, Fluka) is poured inside the pre-separator. A coating of 1% (*w*/*v*) solution of silicon oil in hexane is used on the impaction plates to prevent particle bounce and re-entrainment. A capsule filled with particles is loaded into a Rotahaler® (Glaxo) which is used as the inhaler to aerosolize the particles. An actuation time of 20 s is allowed for each capsule to completely disperse all the particles. Each experiment is repeated at least three times. Statistical analysis of the results is performed by ANOVA.

Particles remaining in the capsule and inhaler device as well as those deposited in the throat, pre-separator, individual impaction plates, and stages are extracted using dilute acidic solution (2% HNO_3). The extracted solutions from different regions are then quantified with inductively coupled plasma (Optica 2000 DV; for Ca^{2+} element). The temperature and relative humidity of the surrounding environment are also measured before each experiment.

The ACI experimental results are characterized by two parameters, emitted dose (ED) and fine particle fraction (FPF). ED is defined as the mass percentage of particles leaving the inhaler (i.e., total amount excluding those in the inhaler and capsule). As particles are discharged from the capsule, a fraction of the particles will be dispersed and flow with the gas stream. Some of the particles in the inhaler will be picked up and entrained by the gas flow, while the rest of the particles will remain in the inhaler and the capsule. Therefore, ED can be considered to account for both aerosolization property and flowability of the particles.

FPF is defined as the amount of the particles deposited in stage 2 or lower in the cascade impactor (particles <5.8 μm) as a percentage of the particles collected from all the parts of the impactor including the inhaler device and capsule. FPF is a commonly used index to represent deposition properties of aerosol particles. Particles that have less deposition at the initial regions and able to reach the lower stages of the impactor would have higher FPF.

RESULTS AND DISCUSSION

Particle Characteristics

The SEM images and size distributions of the different particle samples used in this study are shown in Fig. 1. Particle size measurement of the non-spherical particles is always a challenge especially with the use of one single parameter. Two most common methods for particle size measurement, laser diffraction measurement and direct visualization from microscopy images, are used in this study. The laser diffraction measurement takes into account the lights diffracted from the dispersed particles to estimate the particle size. However, the diffracted lights can change with the orientation of non-spherical particles, and the results may not be a good representation of the actual size. Therefore, particle size obtained from SEM images is also used for comparison with laser diffraction measurement.

It is to note that the size distributions obtained from laser diffraction measurement are volume-weighted, while the size distributions from the SEM images are number-weighted. Therefore, the SEM size distributions are converted to volume-weighted distribution before comparisons are made. The conversion of number-weighted size distribution to volume-weighted size distribution requires the knowledge of particle volume. Therefore, pollen-shaped particle volume is assumed to be the same as a sphere with the same diameter. Plate-shaped particle volume is assumed to be the same as a

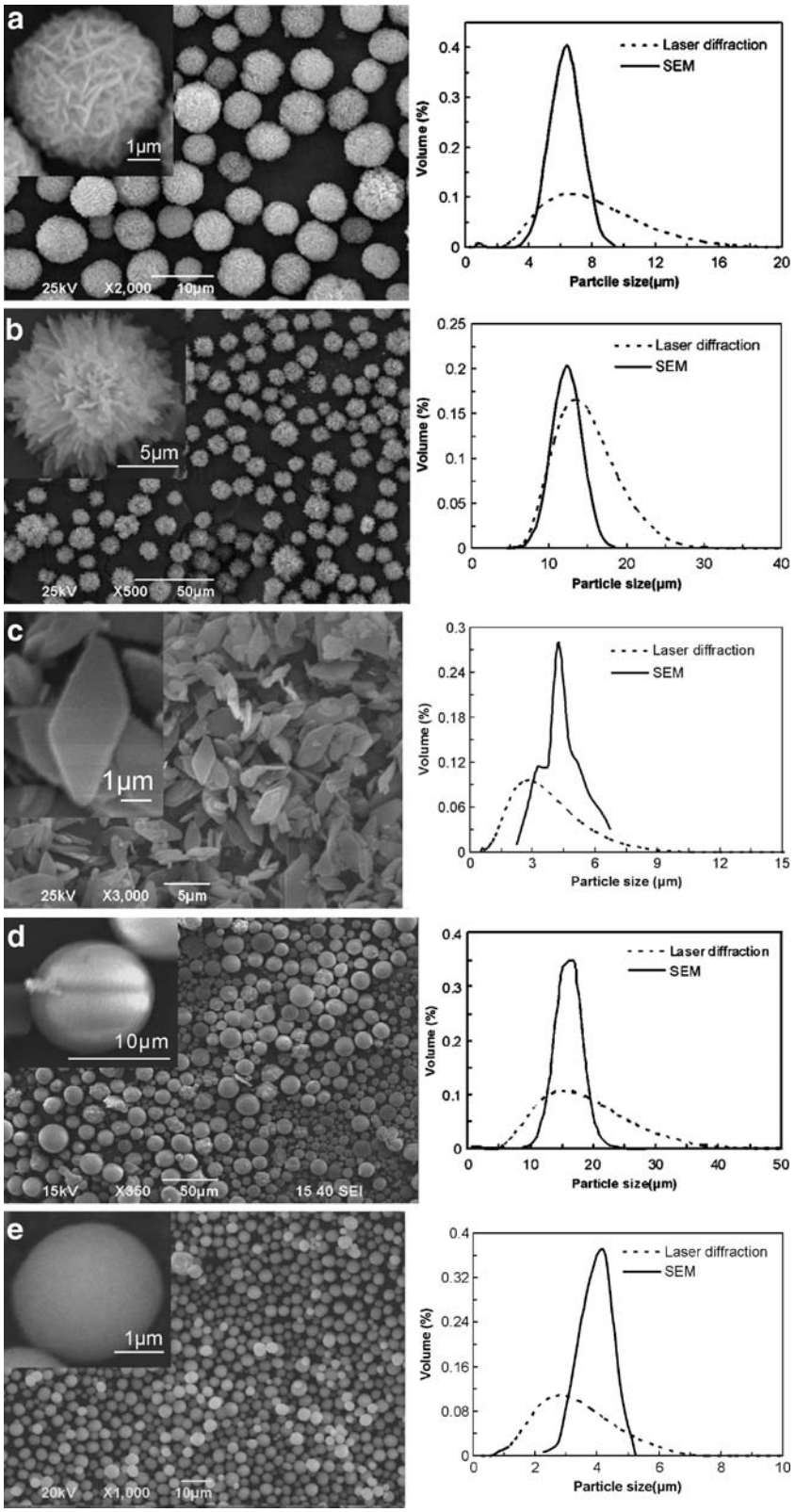

Fig. 1. SEM image and size distribution of **a** pollen-shaped I HA particles; **b** pollen-shaped II HA particles; **c** spherical I $CaCO_3$ particles; **d** spherical II HA particles; **e** plate-shaped CaC_2O_4 particles; **f** cube-shaped $CaCO_3$ particles; **g** needle-shaped $CaCO_3$ particles

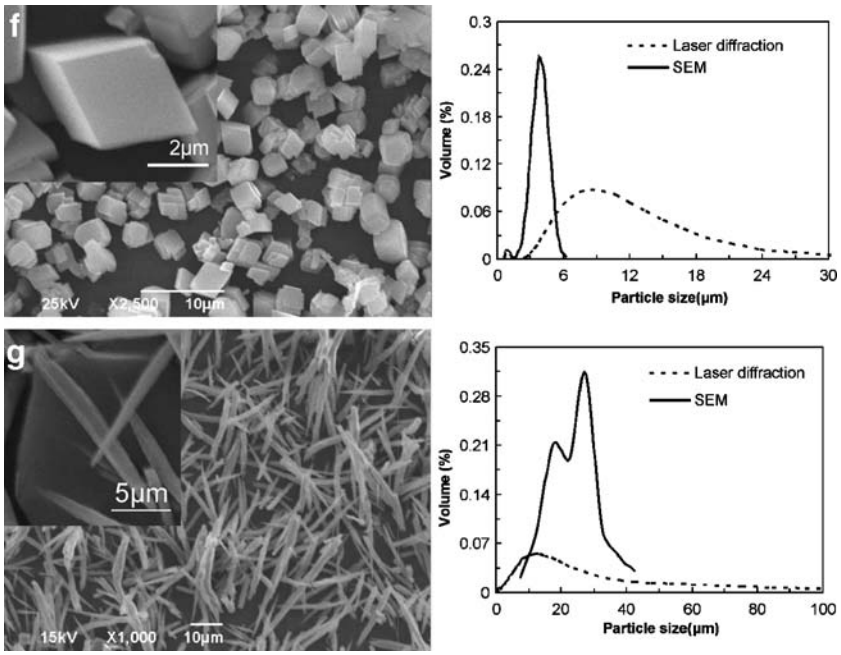

Fig. 1. (continued)

particle that has the average width and thickness from SEM images. Volume of cube-shaped particle is calculated as the cube of the side length. Needle-shaped particle volume is assumed to be the same as a cylinder with the same length and average diameter from SEM images. The physical properties of the particles are listed in Table I.

Two types of pollen-shaped particles are produced. The HA particles synthesized with PSS concentration of 40 g/l and urea concentration of 7.5 M (Fig. 1a, pollen-shaped I) has a petal-like surface structure and a d(50%, SEM) of 6.3 μm (18). The HA particles synthesized with PSS concentration of 40 g/l and urea concentration of 3 M (Fig. 1b, pollen-shaped II) has a fibrous surface structure and a d(50%, SEM) of 12.5 μm. As shown in Fig. 1a, b, both laser diffraction and SEM measured size distributions yield similar mode, but the laser diffraction measurement consistently gives a larger size distribution than the SEM measurement. This maybe because the surface irregularity of both pollen-shaped HA particles causes additional diffraction of the light beam in laser diffraction measurement and yields a larger measurement size than the actual size. Therefore, the SEM image measurement results are used as the characteristic size.

The size of spherical particles does not vary with the particle orientation. The size distribution of the spherical particles obtained by laser diffraction is indeed similar to the size obtained from SEM images shown in Fig. 1c, d. Spherical $CaCO_3$ (spherical I) sample in Fig. 1c has a d(50%, SEM) of 3.7 μm and a d(50%, LD) of 3.9. The larger spherical HA sample (spherical II), produced with PSS concentration of 80 g/l and urea concentration of 7.5 M, has a d(50%,SEM) of 15 μm and a d(50%, LD) of 14.9 μm. Both SEM and LD measurements give similar d(50%) for the spherical particles. Since LD takes a larger sample size into consideration, LD measurement size is taken as the characteristic size.

The plate-shaped particles can be described by three dimensions, length (maximum dimension), width (intermediate dimension), and height (minimum dimension). The SEM image and size distributions of the plate-shaped particles are shown in Fig. 1e. Since the laser diffraction measurement depends on the particle orientation, it would be difficult to

Table I. Properties of Different Shape Particles

Shape	d(50%, LD) (μm)	d(50%, SEM) (μm)	ρ_{bulk} (g/cm^3, n=0)	ρ_{tap} (g/cm^3, n=2,500)	CI (%)	Angle of slide, θ (deg)
Pollen-shaped (I)	6.7	6.3	0.35	0.72	51.8±3.6	35.3±2.3
Pollen-shaped (II)	13.4	12.5	0.23	0.40	42.2±2.9	34.7±0.6
Spherical I	3.9	3.7	0.58	1.04	44±3.1	65.0±3.0
Spherical II	14.9	15	1.054	1.13	19.2±1.3	49.3±2.6
Plate-shaped	2.8	4.2 (length) 2.0 (width) 0.5 (thickness)	0.39	0.66	40.6±2.8	51±6.1
Cube-shaped	8.5	3.7	0.29	0.62	53.6±3.8	55.7±5.5
Needle-shaped	11.6	24.1 (length) 1.9 (diameter)	0.28	0.46	39.9±2.8	40.7±1.5

judge the true representation of the laser diffraction measured size distribution. Therefore, it is more appropriate to use the d(50%, SEM) of the length (4.2 μm) as the characteristic size of plate-shaped particles. The calculation of the aerodynamic diameter requires the volume equivalent diameter which is estimated from the dimensions obtained from SEM measurements.

The SEM image and size distributions of the cube-shaped $CaCO_3$ particles are shown in Fig. 1f. The laser diffraction measurement yields a d(50%) of 8.5 μm, while SEM measurement shows that the cubes has a side length of 3.7 μm. The SEM image shows that the cube-shaped particles are clustered together. In this case, the laser diffraction would give a better measurement of the average cluster size than the side length obtained from SEM measurement. Therefore, the size obtained from the laser diffraction is used as the characteristics size and volume equivalent diameter for cube-shaped particles.

The SEM image and size distributions of needle-shaped $CaCO_3$ particles are shown in Fig. 1g. d(50%) of the needle-shaped $CaCO_3$ particles from laser diffraction is 11.6 μm. It is obvious from the SEM image that most of the particles have a length of over 20 μm and a diameter of around 2 μm. In this case, it is quite possible that the laser diffraction measurement result comprises measurements of both the length and diameter of the needle-shaped particle. Therefore, the d (50%, SEM) of 24.1 μm is used instead as the characteristic size of the needle-shaped particles. Aerodynamic diameter is estimated from the dimensions from SEM measurements. The characteristic sizes of different shape particles are listed in Table II.

Shape Factor of the Different Shape Particles

The determination of the aerodynamic diameter requires the dynamic shape factor of the particles, which is a function of the drag force experienced by the moving particles. The dynamic shape factor for sphere is defined as 1. However, for irregular shape particles, it is difficult to measure the dynamic shape factor. Therefore, the shape factors of the particles are estimated based on Davies (28) in which shape factors for different shape particles are extensively reviewed.

A needle shape can be viewed as a prolate spheroid (polar diameter greater than equatorial diameter) with a very high aspect ratio. The shape factors of prolate spheroids were reported to be between 1 and 15.43 for aspect ratios range from 1 to 1,000 (28). An increase in the aspect ratio would increase the shape factor. The needle-shaped particles used in this study have an average aspect ratio of 12.7 (average length 24.1 μm and average width 1.9 μm). Thus, the average dynamic shape factor is estimated to be 1.7 by interpolation.

The plate-shaped particles, on the other hand, can be considered as an oblate spheroid (polar diameter shorter than equatorial diameter). The dynamic shape factor of an oblate spheroid with an aspect ratio of 10 is reported to be 1.49 (28). Since the aspect ratio of the plate-shaped particles used is around 10, a dynamic shape factor of 1.5 can be estimated.

For the cube-shaped particles, SEM images indicate that the particles are clustered together and form rock-shaped clusters. The dynamic shape factor of rock-like quartz particles is found to be 1.36 (28). From the SEM image, it can be seen that these particles are closer to spherical shape than the rock-like quartz particles. Thus, these cube-shaped clusters are estimated to have a shape factor of 1.3.

The pollen-shaped particles closely resemble a spherical shape. The rough surface would cause a slightly higher shape factor than spherical particles. Thus, a dynamic shape factor of 1.2 is estimated for the pollen-shaped particles.

It is also to note that the dynamic shape factors are to be used in the calculation of aerodynamic diameter. While the aerodynamic diameter is proportional to the square root of the dynamic shape factor, the error in the estimation of dynamic shape factor should have a relatively small impact on the accuracy of the aerodynamic diameter calculated. Aerodynamic diameter of the different shape particles are calculated from Eq. 1. The calculated aerodynamic diameters for the particles are also shown in Table II.

Table II. Characteristic Size, Shape Factor, and Aerodynamic Diameter of Different Shape Particles

Shape	Characteristics size (μm)	Shape factor, λ (−)	Aerodynamic diameter, d_a (μm)
Pollen-shaped I	6.3	1.2	4.1
Pollen-shaped II	12.5	1.2	5.9
Spherical I	3.9	1.0	3.8
Spherical II	14.9	1.0	15.9
Plate-shaped	4.2	1.5	1.4
Cube-shaped	8.5	1.3	3.2
Needle-shaped	24.1	1.7	2.7

Flowability, Aerosolization, and Deposition Properties

CI, θ, ED, and FPF results of the different shape particles are plotted as a function of their aerodynamic diameter and characteristic size in Fig. 2a, b, respectively. The aerodynamic diameter of the particles ranges from 1.4 to 15.8 μm, with a majority of particles in the range of 1.4–5.9 μm. The different shape particles have their characteristic size ranging from 3.9 to 24.1 μm. The flowability, aerosolization, and deposition properties show no evidence of direct relation with the aerodynamic diameter as well as the particle characteristic size. Therefore, the inhalation properties of the particles will need to be analyzed separately according to either the aerodynamic diameter or the characteristic size.

Aerodynamic diameter takes into account the difference in particle size, density, and shape. It is also a commonly accepted way of categorizing aerosol particles. Therefore, the particles used in this study are grouped into three aerodynamic diameter ranges. The CI,θ, ED, and FPF results of the different shape particles in the respective aerodynamic diameter ranges are shown in Fig. 3. Other than spherical II particles, the aerodynamic diameter of all the particles used are within a narrow range of about 1.4–5.9 μm. The p values of the statistical analysis within each size group are also presented in the figure. The difference among the experimental results within each size group can be considered statistically significant for $p<0.05$ (29).

Needle-shaped and plate-shaped particles are in the similar d_a range of 1.4–2.7 μm. In this size range, both plate-shaped and needle-shaped particles show comparable CI and

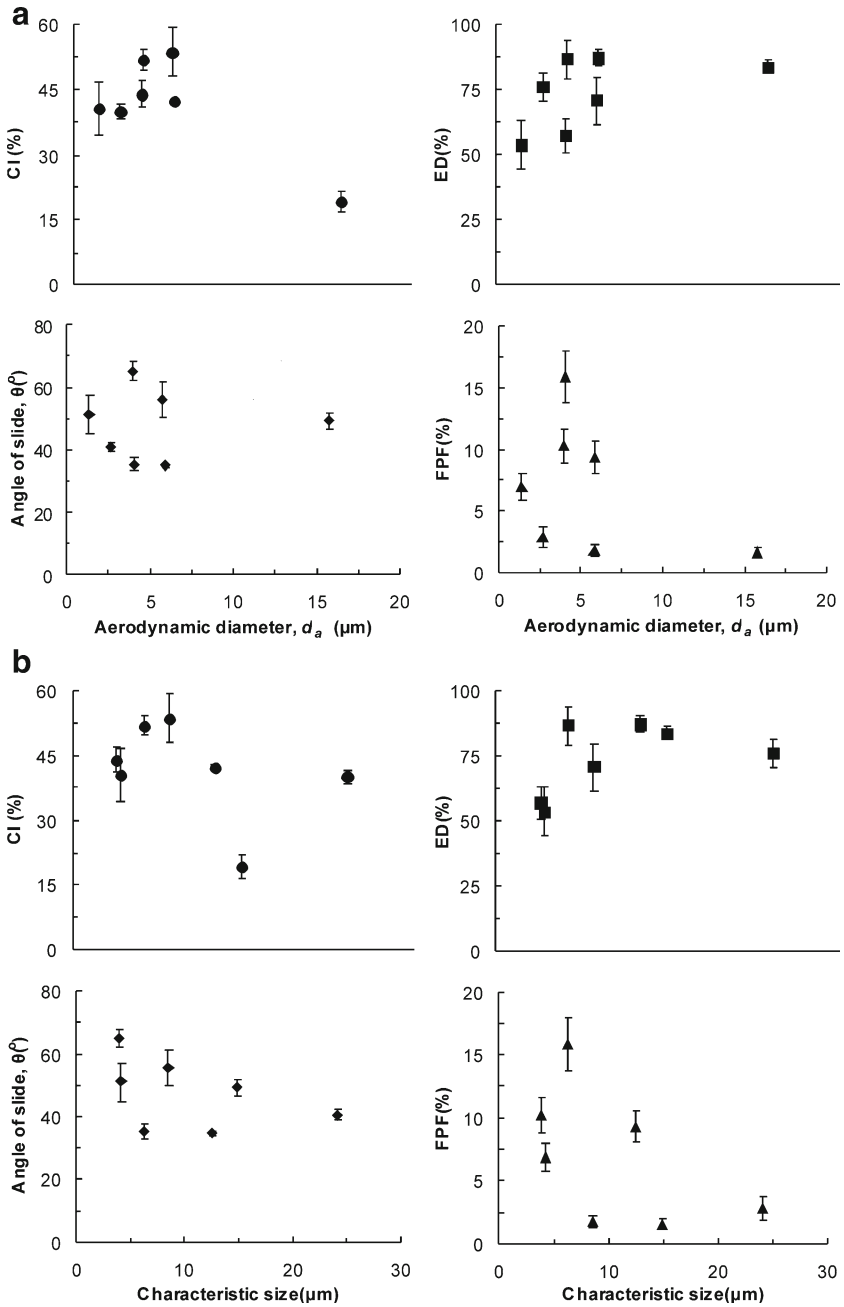

Fig. 2. CI, θ, ED, and FPF results of different shape particles as a function of their **a** aerodynamic diameter and **b** characteristic size (*error bars* indicate standard deviation, n=3)

θ. Generally, CI of 25 and above indicates poor flow and 15 and below indicates good flow (30). In this study, most of the particles used are observed to have high CI. Both needle-shaped and plate-shaped particles have high CI of around 40. Because of the flat surfaces, the contact surface areas of these particles are large. The particles would experience high interparticle forces and form aggregates. Their high CI would be a reflection of the breakage of the aggregates and rearrangement of particles (25). The aggregation tendency of the particles causes high resistance to flow; thus, high θ is also observed. However, though the particles show similar flowability, needle-shaped particles have a higher ED than the plate-shaped particles. Even though both particles have similar aerodynamic diameter, in fact, the needle-shaped particles have much higher characteristic size than the plate-shape particles. Therefore, the needle-shaped particles should have lower interparticle interaction and showed lower cohesiveness than the plate-shaped particles. As shown from the regional deposition results in Fig. 4, larger amount of the plate-shaped particles would be deposited in the inhaler region compared to needle-shaped particles. Despite the fact that plate-shaped particles have lower ED than needle-shaped particles, they exhibit higher FPF. It indicates that even though the needle-shaped particles are easier to be aerosolized than the plate-shaped particles, the relatively large major dimension of the needle-shaped particles makes them more susceptible to early deposition because of interception deposition mechanism (10).

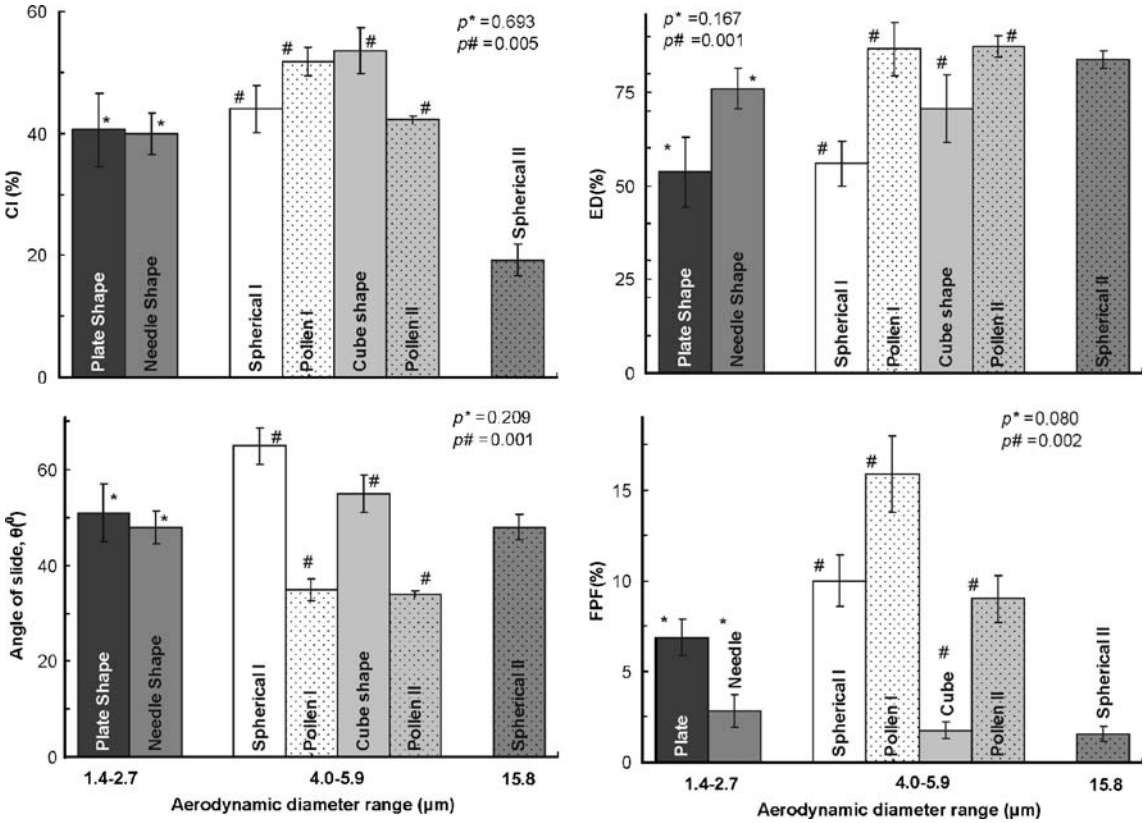

Fig. 3. CI, θ, ED, and FPF results of different shape particles in similar aerodynamic diameter range (*error bars* indicate standard deviation, $n=3$)

Spherical I, pollen-shaped I, cube-shaped, and pollen-shaped II particles have comparable d_a in the range of 4.0–5.9 μm. CI results indicate that spherical I and pollen-shaped II would have better flowability than cube-shaped and pollen-shaped I particles. However, θ results show that both pollen-shaped I and pollen-shaped II particles can flow better than spherical I and cube-shaped particles. Since CI makes use of the difference in tap density and bulk density, high CI can indicate weak interparticle forces being overcome by tapping. The weak interparticle forces may lead to good flowability, as indicated by the contradicting behavior in CI and θ of pollen-shaped I particles. It is possible that the surface features of the pollen-shaped particles increase the distance between two interacting particles and reduce their contact surface. Thus, the interparticle forces would be lower. The low interparticle forces of pollen-shaped particles also lead to better ED than cube-shaped and spherical I particles. Both pollen-shaped particles have an excellent ED of 86–88%. However, because of the large characteristic size, pollen-shaped II particles have higher deposition in the pre-separator and lower FPF is

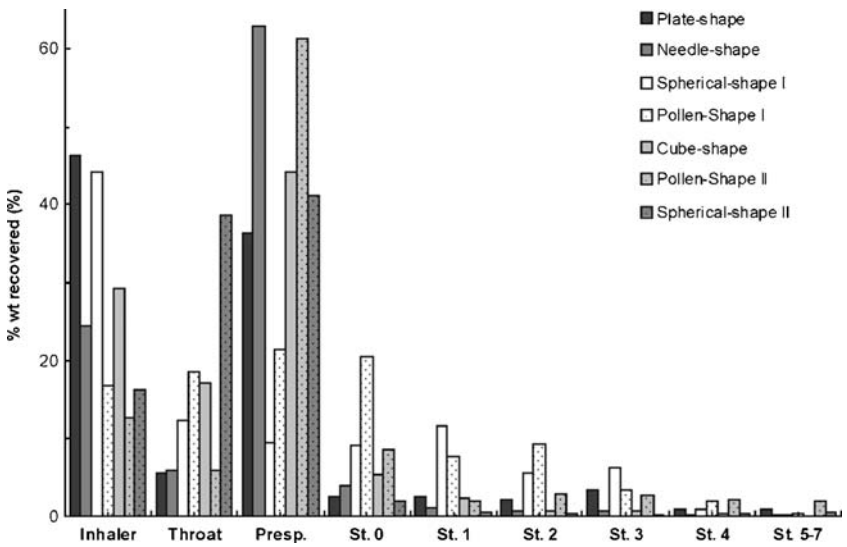

Fig. 4. Regional deposition in the Andersen cascade impactor for different shape particles

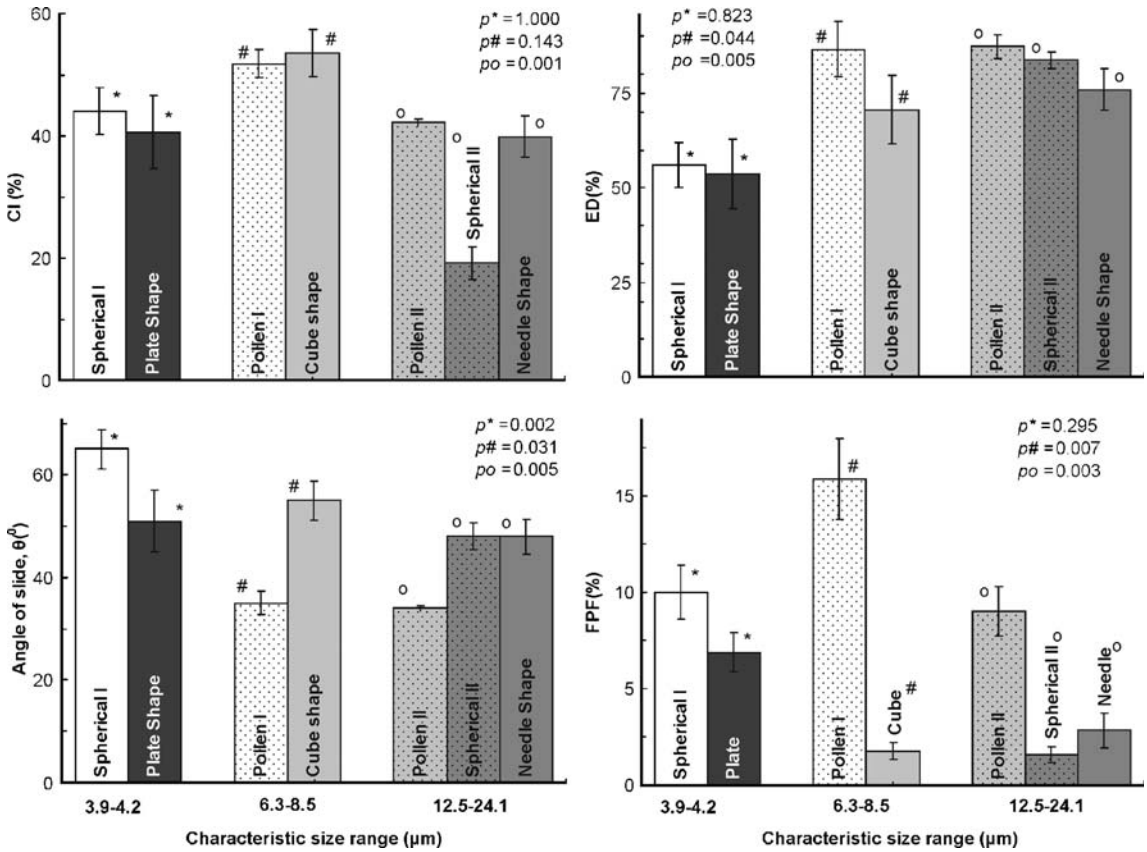

Fig. 5. CI, θ, ED, and FPF results of different shape particles in similar characteristic size range (*error bars* indicate standard deviation, $n=3$)

observed compared to pollen-shaped I particles. On the other hand, cube-shaped and spherical I particles show poor flowability in both CI and θ. Therefore, it is believed that the interparticle forces are stronger for cube-shaped than for spherical I particles. The strong interparticle forces also result in low ED of both particles. However, a big difference between the spherical I and the cube-shaped particles is that despite a low ED, spherical I particles can still give a relatively high FPF. Since the cube-shaped particle possesses large characteristic size, most of them are deposited in the pre-separator and the initial stages of the impactor and a less amount can go to the lower stages.

The spherical II particles have an average d_a of 15.8 μm, much higher than other particles. As expected, the large size favors better CI, θ, and ED. However, deposition due to inertial impaction and interception in the throat and pre-separator are also increased. Therefore, the low FPF is observed for the spherical II particles.

The physical size of particles also plays a vital role in the flow, aerosolization, and dispersion behavior. Figure 5 shows the CI, θ, ED, and FPF results of the different shape particles grouped in similar characteristic size range. It can be seen that the grouping of particles based on characteristic size is different from that based on aerodynamic diameter. Spherical I and plate-shaped particles are in a smaller size range of 3.9–4.2 μm, pollen-shaped I and cube-shaped particles are in a medium size range of 6.3–8.5 μm, and pollen-shaped II, spherical II, and needle-shaped particles are in a large size range of 12.5–24.1 μm.

The physical size of the particles would be closely related to the interparticle forces as well as the deposition mechanism

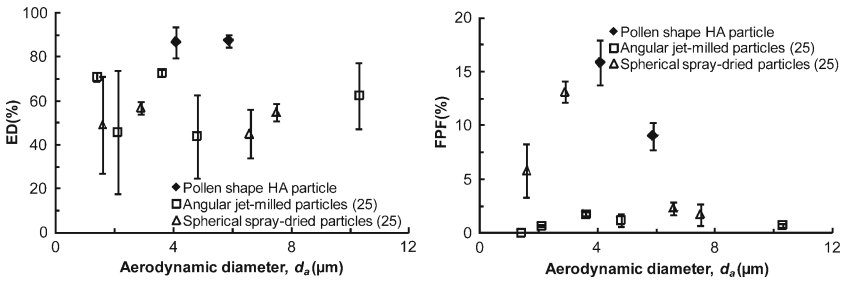

Fig. 6. Comparison of **a** ED and **b** FPF of pollen-shaped HA particles with angular jet-milled and spherical spray-dried particles (*error bars* indicate standard deviation)

in the cascade impactor. In general, small physical size would have stronger interparticle forces than inertial forces within the size range of 1–10 μm (25). The strong interparticle forces would reduce the particle flowability. Therefore, large particles generally have higher ED. On the other hand, large particles are more susceptible to early deposition due to inertial impaction and interception, and low FPF is observed. As shown in Fig. 5, both flowability (in terms of θ) and ED follow a general increase with an increase in particle characteristic size, while FPF follows a general decrease with an increase in particle characteristic size with the exception of both pollen-shaped particles. In both medium and large characteristic size range, both pollen-shaped particles show superior θ, ED, and FPF. The FPF of pollen-shaped II is even comparable to the much smaller sized spherical I particles. As discussed in the earlier section regarding aerodynamic diameter, the pollen-shaped structure minimizes the interparticle forces and aggregation tendency. It would be easier to disperse and deliver pollen-shaped particles in dry powder inhalation.

Comparison with Literature Results

There are limited ED and FPF results in the literature using single particle formulation in cascade impactor. The ED and FPF of both pollen-shaped I and pollen-shaped II particles are compared with angular jet-milled and spherical spray-dried mannitol particles with aerodynamic diameter lower than 10 μm (25). The mannitol particles were aerosolized at an air flow rate of 60 l/min with an actuation time of 20 s, whereas the flow rate used in this study is 30 l/min with the same actuation time. It can be seen in Fig. 6 that despite the lower air flow rate, the pollen-shaped I and pollen-shaped II particles show higher ED and FPF than the angular and spherical particles of similar size (aerosolized by Rotahaler®). One of the spherical particles indeed showed higher FPF than the pollen-shaped particles. However, the spherical particles have an average size of 2.9 μm, which is much smaller than the 6.3- and 12.5-μm pollen-shaped particles. It is believed that the high FPF is not contributed from the spherical shape. Pollen-shaped particles having similar size as the spherical particles are anticipated to have higher FPF based on the comparison of similar-sized particles used in this study. An increase in flow rate can substantially increase the total particle emission from an inhaler (31). It is expected that pollen-shaped I and pollen-shaped II particles would exhibit a higher ED and FPF at a flow rate of 60 l/min. Based on the results of this study, it can be shown that the use of pollen-shaped particles would be promising in improving the delivery efficiency of dry particle inhalations.

CONCLUDING REMARKS

The flow and deposition properties of different shape particles are investigated. Since there is no good parameter to account for particle shape, the different particles are compared against both characteristic size and aerodynamic diameter. It can be seen in this study that even within the d_a range of 1–5 μm, the FPF can vary substantially from 2% to 16% depending on the shape of the particles. It is found that particle shape has a strong effect on particle behavior. Careful control of the shape can improve the flowability, aerosolization, and deposition performance of the particles. Pollen-shaped particles are found to exhibit better flowability, aerosolization, and deposition properties compared with other particle shapes. The use of pollen-shaped drugs can be a good solution to improve the delivery efficiency in dry particle inhalation.

ACKNOWLEDGMENT

The authors are grateful to the financial support of NTU/SUG grant. The authors would also like to express their appreciation to Prof. Xu Rong and Dr. Yongsheng Wang for their help in particle synthesis.

REFERENCES

1. Edwards DA. Delivery of biological agents by aerosols. AIChE J. 2002;48:2–6.
2. Hickey AJ. Pharmaceutical inhalation aerosol technology, vol. 134. New York: Marcel Dekker; 2004.
3. Crowder TM, Rosati JA, Schroeter JD, Hickey AJ, Martonen TB. Fundamental effects of particle morphology on lung delivery: predictions of Stokes' law and the particular relevance to dry powder inhaler formulation and development. Pharm Res. 2002;19:239–45.
4. Hinds WC. Aerosol technology: properties, behavior, and measurement of airborne particles. New York: Wiley; 1982.
5. Baron PA, Willeke K. Aerosol measurement: preinciples, techniques and applications. 2nd ed. NewYork: Willy-Interscience; 2001.
6. Tang P, Chan HK, Raper JA. Prediction of aerodynamic diameter of particles with rough surfaces. Powder Technol. 2004;147:64–78.
7. Chan H-K, Gonda I. Aerodynamic properties of elongated particles of cromoglycic acid. J Aerosol Sci. 1989;20:157–68.
8. Fults KA, Miller IF, Hickey AJ. Effect of particle morphology on emitted dose of fatty acid-treated disodium cromoglycate powder aerosols. Pharm Dev Technol. 1997;2:67–79.
9. Larhrib H, Martin GP, Prime D, Marriott C. Characterisation and deposition studies of engineered lactose crystals with potential for use as a carrier for aerosolised salbutamol sulfate from dry powder inhalers. Eur J Pharm Sci. 2003;19:211–21.
10. Balásházy I, Martonen TB, Hofmann W. Fiber deposition in airway bifurcations. J Aerosol Med. 1990;3:243–60.
11. Otsuka A, Iida K, Danjo K, Sunda H. Measurement of the adhesive forces between particles of powdered materials and a glass substrate by means of the impact separation method. II. Effects of particle shape and surface asperity. Chemical & Pharmaceutical Bulletin. 1988;36:741–9.
12. Visser J. Van der waals and other cohesive forces affecting powder fluidization. Powder Technol. 1989;58:1–10.
13. Zimon AD. Adhesion of dust and powder. 2nd ed. London: Consultant Bureau; 1982.
14. Mullins ME, Michaels LP, Menon V, Locke B, Ranade MB. Effect of geometry on particle adhesion. Aerosol Sci Tech. 1992;17:105–18.
15. Bailey AG. Electrostatic phenomena during powder handling. Powder Technol. 1984;37:71–85.
16. Karra VK, Fuerstenau DW. The effect of humidity on the trace mixing kinetics in fine powders. Powder Technol. 1977;16:97–105.
17. Zeng XM, Martin GP, Marriott C, Pritchard J. The influence of carrier morphology on drug delivery by dry powder inhalers. Int J Pharm. 2000;200:93–106.
18. Hassan MS, Lau R. Pollen shape particles for pulmonary drug delivery: in vitro study of flow and deposition properties. 13th International Conference on Biomedical Engineering, Springerlink; 2009. p. 1434–7

19. Wang Y, Gunawan P, Xu R. Polyelectrolyte-mediated formation of hydroxyapatite microspheres: from anisotropic to isotropic growth. J Colloid Interface Sci. 2009;339:69–77.
20. Wang C, He C, Tong Z, Liu X, Ren B, Zeng F. Combination of adsorption by porous $CaCO_3$ microparticles and encapsulation by polyelectrolyte multilayer films for sustained drug delivery. Int J Pharm. 2006;308:160–7.
21. Yu J, Tang H, Cheng B, Zhao X. Morphological control of calcium oxalate particles in the presence of poly-(styrene-alt-maleic acid). J Solid State Chem. 2004;177:3368–74.
22. Yu J, Lei M, Cheng B, Zhao X. Facile preparation of calcium carbonate particles with unusual morphologies by precipitation reaction. J Cryst Growth. 2004;261:566–70.
23. Lucas A, Gaudé J, Carel C, Michel J-F, Cathelineau G. A synthetic aragonite-based ceramic as a bone graft substitute and substrate for antibiotics. Int J Inorg Mater. 2001;3:87–94.
24. Shi L, Plumley CJ, Berkland C. Biodegradable nanoparticle flocculates for dry powder aerosol formulation. Langmuir. 2007;23:10897–901.
25. Louey M, Van Oort M, Hickey A. Aerosol dispersion of respirable particles in narrow size distributions produced by jet-milling and spray-drying techniques. Pharm Res. 2004;21:1200–6.
26. Louey M, Van Oort M, Hickey A. Aerosol dispersion of respirable particles in narrow size distributions using drug-alone and lactose-blend formulations. Pharm Res. 2004;21: 1207–13.
27. Larhrib H, Martin GP, Marriott C, Prime D. The influence of carrier and drug morphology on drug delivery from dry powder formulations. Int J Pharm. 2003;257:283–96.
28. Davies CN. Particle–fluid interaction. J Aerosol Sci. 1979;10:477–513.
29. Sung J, Padilla D, Garcia-Contreras L, VerBerkmoes J, Durbin D, Peloquin C, *et al.* Formulation and pharmacokinetics of self-assembled rifampicin nanoparticle systems for pulmonary delivery. Pharm Res. 2009;26(8):1847–55.
30. Kanig JL, Lachman L, Lieberman HA. The theory and practice of industrial pharmacy. 3rd ed. Philadelphia: Lea & Febiger; 1986.
31. French DL, Edwards DA, Niven RW. The influence of formulation on emission, deaggregation and deposition of dry powders for inhalation. J Aerosol Sci. 1996;27:769–83.